Thermoelectric properties of $Ni_{0.05}Mo_3Sb_{5.4}Te_{1.6}$ composites with NiSb nanocoating

Nagaraj Nandihalli, Robert Liang, Dimuthu Wijethunge, Norman Zhou, and Holger Kleinke

Citation: AIP Advances **8**, 125304 (2018); doi: 10.1063/1.5038675
View online: https://doi.org/10.1063/1.5038675
View Table of Contents: http://aip.scitation.org/toc/adv/8/12
Published by the American Institute of Physics

Articles you may be interested in

Effective degradation of oil pollutants in water by hydrodynamic cavitation combined with electrocatalytic membrane
AIP Advances **8**, 125308 (2018); 10.1063/1.5028152

Mechanical properties of bi- and poly-crystalline ice
AIP Advances **8**, 125108 (2018); 10.1063/1.5042725

Influence of trace water on decomposition mechanism of c-C_4F_8 as environmental friendly insulating gas at high temperature
AIP Advances **8**, 125202 (2018); 10.1063/1.5044751

Evolution of incipient cavitation around two cylinders with different headforms
AIP Advances **8**, 125307 (2018); 10.1063/1.5045312

First-principles study of structural phase transformation and dynamical stability of cubic AlN semiconductors
AIP Advances **8**, 125006 (2018); 10.1063/1.5054697

Evaporation-induced assembly of colloidal clusters into superclusters with nonconvex deltahedral geometry
AIP Advances **8**, 125116 (2018); 10.1063/1.5055638

Thermoelectric properties of $Ni_{0.05}Mo_3Sb_{5.4}Te_{1.6}$ composites with NiSb nanocoating

Nagaraj Nandihalli,[1,2,a] Robert Liang,[2,3] Dimuthu Wijethunge,[4] Norman Zhou,[2,3] and Holger Kleinke[1,2]

[1]*Department of Chemistry, University of Waterloo, Waterloo, Ontario N2L 3G1, Canada*
[2]*Waterloo Institute for Nanotechnology, University of Waterloo, Waterloo, Ontario N2L 3G1, Canada*
[3]*Center of Advanced Materials Joining, Department of Mechanical and Mechatronics Engineering, University of Waterloo, Waterloo, Ontario N2L 3G1, Canada*
[4]*Center for Advanced Mechatronics Systems, University of Moratuwa, Sri Lanka*

(Received 4 May 2018; accepted 23 October 2018; published online 4 December 2018)

NiSb nanoparticles by 0.034, 0.074 and 0.16 volume fractions were successfully coated on bulk polycrystalline $Ni_{0.05}Mo_3Sb_{5.4}Te_{1.6}$ thermoelectric (TE) particles through a solvothermal route without deteriorating the bulk $Ni_{0.05}Mo_3Sb_{5.4}Te_{1.6}$ material. The samples were consolidated through hot pressing and their thermoelectric (TE) properties were characterized. At 400 K, 500 K, and 600 K, 0.074 NiSb sample exhibited 22%, 16% and 11.3% increases in the power factor (*P.F.*) compared to bulk material. The main contributing factor to this enhanced power factor is the elevated electrical conductivity. For the same sample, the reciprocal relationship between Seebeck coefficient and electrical conductivity is decoupled. Sample 0.16 NiSb exhibited the highest electrical conductivity among the three samples. The thermal conductivity of the 0.16 sample was less temperature sensitive compared to other samples. HRTEM and SEM tools were applied to comprehend microstructural features and their relationship to TE transport properties. Pore effect on the thermal and electrical conductivity was elucidated. This study shows that grain-boundary manipulation via this wet chemistry technique is indeed an economically viable method to fabricate and optimize the transport properties of bulk TE materials. © *2018 Author(s). All article content, except where otherwise noted, is licensed under a Creative Commons Attribution (CC BY) license (http://creativecommons.org/licenses/by/4.0/).* https://doi.org/10.1063/1.5038675

INTRODUCTION

Rapid progress in nanotechnology tools has given new dimensions to energy harnessing materials. One such beneficiary is thermoelectric (TE) materials.[1–3] These semiconducting materials convert thermal energy into electrical energy when a certain temperature difference is established between two ends of the material (power generation mode), or they can maintain a temperature difference between two ends of the material when electrical energy is supplied to them (cooling mode). In 2015, world-wide usage of vehicles including cars, trucks, and buses exceeded 1 billion and is expected rise in the coming years.[4] The wasted heat from vehicle's exhaust and radiators is enormous. If this wasted heat could be extracted and converted into electrical energy using TE devices, fossil-fuel consumption and carbon emission could be reduced on a large scale.

A parameter called figure-of-merit (ZT) describes the conversion efficiency of a TE material and is given by $ZT = S^2\sigma\ \kappa^{-1}T$, where S is the Seebeck coefficient, σ is the electrical conductivity, κ is the thermal conductivity, and T is the operating temperature. However balancing the electrical and thermal properties is very challenging as both thermal and electrical transport properties are strongly coupled.[2] Synthesizing a nanocomposite with already promising TE material as a starting

[a]Corresponding author nnandiha@uwaterloo.ca

 © Author(s) 2018

material is getting more attention.[5–9] The lattice component of thermal conductivity, κ_l, is defined by the Boltzmann equation under relaxation time approximation and is given by, $\kappa_l = (1/3)C_v l v$, where v is the phonon group velocity, C_v is the specific heat, and l is the phonon free path. Among these parameters controlling l is the most fruitful option as many investigations show.[2,10] Reducing the mean free path results in reduction of κ, which in turn elevates the figure-of-merit, provided the electrical conductivity and the Seebeck coefficient are unaffected. In typical nanocomposite synthesis, chemically and physically stable nanoparticles are mixed with a material having promising TE properties. The materials are consolidated through either hot-pressing or spark plasma sintering.[3] Limitations to these methods include inhomogeneity and instability. In TE nanocomposite materials, the interfaces between bulk particles or at the junction of bulk particles and embedded foreign nanoparticles play a very important role in deciding the overall performance of a TE material.[8] Thus, the techniques used to fabricate the composite materials are critical to achieve optimized transport properties.[8,11]

Interfaces in thermoelectric materials can influence the Seebeck effect due to size quantization effects[12] or due to the energy filtering of low energy charge carriers.[13] Interfaces are also found to reduce thermal conductivity because of diffusive scattering of phonons[14] and play an important role in deciding the electrical conductivity depending on the nature of interfaces. For a fixed Seebeck coefficient, increasing ZT requires that the reduction in mobility due to charge carrier scattering at interfaces is smaller than the proportional reduction in thermal conductivity.[15] There are numerous suggestions on the nature of interfaces, some of them practically viable and many of them still conceptual, such as embedded nanoinclusions, nanocoated bulk grains, polycrystalline microstructure, preferential alignment of grains along favorable transport directions, reduced grain size to facilitate preferential scattering of charge-carriers, coherent inclusion, lamellar/multilayer structures, and nanomeshes.[8,11,16–18] There are several methods that use solution-based nanoparticles for TE nanocomposites.[19–22] Recent reports describe interfacial nanocoating,[23–25] a wet chemistry process where the starting materials and the pulverized bulk material are added to a reaction container such as an autoclave. When the reaction is complete, nanoparticles were found to coat the polycrystalline bulk material. The outcome of that investigation was an enhanced figure-of-merit for $La_{0.9}CoFe_3Sb_{12}$ by 15-30%. Three important conditions need to be fulfilled while executing this nanocoating. Firstly, the coating process should leave the bulk material unaffected. Secondly, the coating needs to be homogeneous. Thirdly, the product needs to be thermodynamically and chemically stable.

In this investigation NiSb nanoparticles were coated on bulk antimonide-telluride ($Ni_{0.05}Mo_3Sb_{5.4}Te_{1.6}$) particles using a simple nanocoating process similar to nanocoating $CoSb_3$ on bulk $CoSb_3$ and $CoSb_3$ on bulk $La_{0.9}CoFe_3Sb_{12}$.[26,27] $Ni_{0.05}Mo_3Sb_{5.4}Te_{1.6}$ has a thermal conductivity of 4.0 W m^{-1} K^{-1} and a ZT of 0.96 at 1000 K.[28] NiSb was chosen because the synthesis process is simple[29,30] and it is smaller in size (60 nm – 80 nm). This grain boundary enhances the surface area (means more interface/unit volume), which aids in phonon scattering. Since NiSb is highly conductive (7.5×10^4 Ω^{-1} cm^{-1} at 325 K)[31] the coating will enhance the electrical conductivity and elevate or leave unaffected the Seebeck coefficient. In addition, bulk NiSb particles (100 μm - 500 μm) have been synthesized and their TE transport properties have been characterized to ascertain their effect on $Ni_{0.05}Mo_3Sb_{5.4}Te_{1.6}$.

EXPERIMENTAL SECTION

The process of synthesizing polycrystalline bulk $Ni_{0.05}Mo_3Sb_{5.4}Te_{1.6}$ through a solid-state reaction can be found in our previous article.[6] In a typical coating process, 2 g of bulk material and the respective amount of starting materials ($NiCl_2{\cdot}6H_2O$ and $SbCl_3$) were added to a Teflon lined autoclave containing 20 mL of ethanol. The mixture was mixed by sonication for 20 minutes. Subsequently, an appropriate amount of $NaBH_4$ was added to a small beaker containing 10 mL of ethanol and sonicated for 10 minutes. The solution containing $NaBH_4$ was added to the autoclave dropwise and left to react for 20 min. The reaction mixture turned into dark black and vigorous effervescence was observed. The amount of starting materials and reducing agent were added in such a way that the end products of the reaction yield would be 0.034, 0.074 and 0.16 NiSb nanoparticles by volume

TABLE I. Experimental densities of bulk and $Ni_{0.05}Mo_3Sb_{5.4}Te_{1.6}$/NiSb composites at 295 K

f	Density of pellet ρ/(g cm^{-3})	Relative density (%)
0 (bulk)	8.0	91.7
0.034	7.8	89.6
0.074:	8.3	95.7
0.160	8.2	94.9

fraction After the reaction, the autoclave was assembled and loaded into an oven. The autoclave was heated slowly to 240 °C and maintained for 72 hours, then allowed to cool down to room temperature naturally. The final product was filtered, washed several times with deionized water and ethanol, and dried under nitrogen atmosphere for 24 hours. The sample with zero volume fraction (f = 0) was retained as a reference sample (bulk sample). The product was subjected to powder XRD for phase analysis using an Inel X-ray diffractometer. The same powder samples were used to study NiSb nanoparticle distribution on bulk particles using a scanning electron microscope (SEM- LEO 1525) equipped with a JEOL JXA-8530F Electron Probe Micro Analyzer (EPMA).

A cylindrical graphite foil was inserted into the bore of a graphite dye. Consolidation of these samples was carried out under uniaxial pressure of 56 MPa at 925 K for two hours with an Oxy-Gon hot press. Throughout the consolidation, the heat zone of the hot press machine was purged with Ar gas. Disks of approximately 2 mm in thickness and 1.27 mm in diameter were obtained. The densities of the discs were measured using the buoyancy method (Table I). Relative density calculations require the maximum theoretical density for composites, which was calculated by the rule of mixtures using the following equation:

$$\text{Composite Density (g cm}^{-3}\text{)} : \text{Volume Fraction of Material 1} \times \text{density of Material 1} + \text{Volume Fraction of Material 2} \times \text{density of Material 2.}$$

The disk-shaped samples were polished with sand paper, then sprayed with graphite on both sides of the disk and transferred to Anter Flashline^{TM} 300 to measure the thermal diffusivity.[32] The thermal diffusivity, α, was measured in an Ar atmosphere between 322 K and 650 K. For each temperature segment, an average of three diffusivity values were taken. The specific heat, C_p, was estimated using the rules of mixture for composite materials:

$$C_p = \sum_{k=1}^{n} C_{pk} m_k \tag{1}$$

Where, C_{pk} is the specific heat of the k^{th} phase and m_k is the mass fraction of the k^{th} phase. Thermal conductivity, κ, was then calculated using $\kappa = \alpha.C_p.\rho$. The disk-shaped samples that were used for diffusivity measurements were cut into quadratic prisms of 2 × 2 × 10 mm using a diamond-saw and used for the simultaneous measurement of the Seebeck coefficient and electrical conductivity between 322K and 755 K. These measurements were performed using ZEM-3 (ULVAC-RIKO, Japan), a commercial four-probe instrument. A -0.09 mm He atmosphere was maintained throughout the measurement.

After hot-press and TE property characterization, the samples were subjected to powder XRD and a high-resolution transmission electron microscope (HRTEM, JEOL 2100F) for grain boundary analysis at McMaster University. For TEM, fine powder of the samples was dispersed on a Cu grid.

RESULTS AND DISCUSSION

The XRD patterns of bulk coated with 0.074 and 0.16 NiSb volume fractions (before hot pressing) are shown in Figure 1(a). As the figure shows, a noticeable NiSb pattern exists for both composites, i.e. as the NiSb content increased the intensity of the NiSb pattern increased. No NiSb peaks were seen in 0.034 NiSb due to the small fraction of NiSb. In addition, no other peaks were observed, indicating that the process of nanocoating did not affect the bulk material.

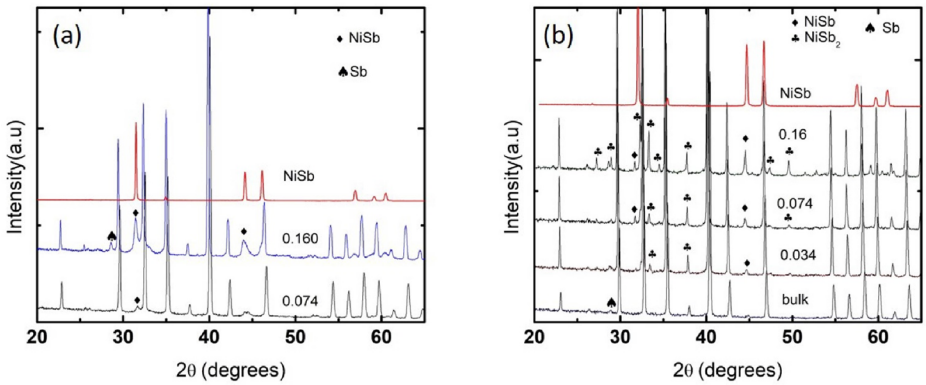

FIG. 1. XRD patterns of NiSb composites and bulk before (a) and after (b) hot pressing.

Figure 1(b) shows the XRD patterns of hot-pressed samples. $NiSb_2$ peaks are evident, with increasing intensities as the fraction of NiSb nanoparticles increases. Since these peaks appeared only after hot pressing, NiSb likely scavenged some Sb from the bulk material during the hot pressing to form $NiSb_2$. From Figure 1(b) it is apparent that after hot press the bulk retained its phase integrity. SEM images of bulk powder coated with NiSb nanoparticles of different volume fractions are exhibited in Figure 2. The images show particles of NiSb are deposited on larger bulk particles. NiSb nanoparticles which were synthesized separately are shown in Figure 2(b). Using the Scherrer equation, the approximate size of NiSb nanoparticles is estimated to be 60 nm – 80 nm.

Figure 3 displays the HRTEM images of hot pressed 0.16 NiSb composites with additional HR images. The unit cell parameters of hexagonal NiSb are 3.939 Å, 3.939 Å, and 5.141 Å. For Mo_3Sb_7, the unit cell parameters are 9.571 Å, 9.571 Å, and 9.571 Å. Needle-like structures in Figure 4(b) are from NiSb and Figure 3(c) and (d) belongs to Mo_3Sb_7.

The temperature dependence of the electrical conductivity is exhibited in Figure 4. The drop in the electrical conductivity as temperature decreases indicates a highly degenerate semiconductor, similar to a family of $Mo_3(Sb,Te)_7$ compounds.[33] For bulk and 0.034 NiSb samples, the electrical conductivity starts at approximately 1322 Ω^{-1} cm^{-1} and shows no significant difference between these samples from 322 K to 755 K. We speculate the volume fraction 0.034 NiSb (7.5×10^4 Ω^{-1} cm^{-1}, inset in Figure 4) should aid in enhancing the electrical conductivity, however this is annulled by the presence of pores and surface area, which are reducing the charge carrier mobility and leaving the electrical conductivity unchanged. At 322 K for the 0.075 NiSb sample, the electrical conductivity jumps to 1901 Ω^{-1} cm^{-1}. This jump can be explained by taking into consideration NiSb cluster formation that provides the least resistive path to charge carriers. In the 0.034 NiSb sample the nanoparticles are randomly coated on bulk particles; they are not connected to each other and therefore there is no change in electrical conductivity. However, as the volumetric content of NiSb is increased, NiSb coated bulk particles make contact with each other, providing a least resistant path to move charge carriers across the material. Similarly, for the 0.16 NiSb sample the electrical conductivity jumps to 2300 Ω^{-1} cm^{-1} at 322 K. In the presence of alloy scattering in the $Mo_3Sb_{7-x}Te_x$ ($0.0 \leq x \leq 1.8$) series of compounds, both conductivity and mobility drop according to $\sigma \sim T^{-0.5}$ and $\mu \sim T^{-0.5}$.[34] Therefore, in bulk and 0.034 NiSb the drop in electrical conductivity must be due to alloy scattering. In 0.074 NiSb and 0.16 NiSb the faster decay in electrical conductivity (deviation from $T^{-0.5}$) is due to mixed scattering. In pure bulk NiSb particles (Figure 4 inset, 100 μm - 500 μm) from 520 K to 710 K, $\sigma \sim T^{-1.0}$, which is a faster decay. Thus, adding increasing amounts of NiSb nanoparticles to bulk material tilts the slope of σ vs. T in 0.074 and 0.16 composites.

Since NiSb nanoparticles were coated on bulk material by a wet chemistry reaction, the porosity effect on the electrical conductivity is of interest. To ascertain the porosity in samples the following equation was used:

$$\sigma_p = \sigma_o(1 - P)/(1 + \beta P) \tag{2}$$

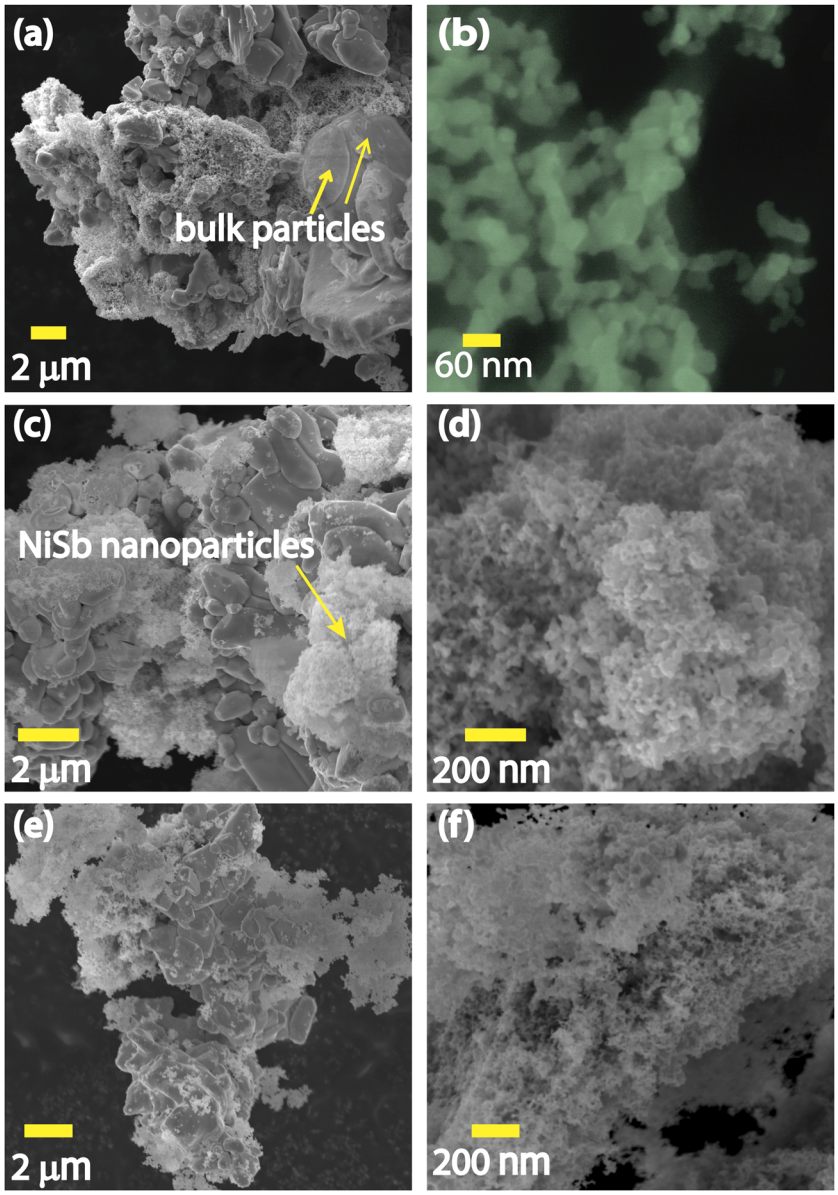

FIG. 2. SEM images of pre-hot-pressed $Ni_{0.05}Mo_3Sb_{5.4}Te_{1.6}$/NiSb powders. (a) 0.034 NiSb nanoparticles on bulk particles; (b) NiSb nanoparticles synthesized separately via solvothermal process; (c) & (d): 0.074 sample; (e) & (f): 0.16 NiSb sample.

Where σ_p is the experimental conductivity with a porosity P, σ_o the theoretical conductivity with zero porosity (the sample is dense and has perfect interfaces), and $\beta = 2$ in the case of spherical pores. Calculated conductivity values are displayed in Figure 5.

For bulk, 0.034, 0.74, and 0.16 samples, the differences in experimental and pore corrected electrical conductivity are listed in Table II. This outcome was expected since for the same samples the relative densities are 91.7%, 89.6%, 95.7%, and 94.9% respectively. In $La_{0.75}Fe_3CoSb_{12}$ there is a systematic reduction in the charge carrier mobility with respect to the amount of porosity. Four samples with 0.3%, 0.5%, 12.4% and 14.8% porosity were found to have mobility of 11.50 $cm^2\ V^{-1}\ S^{-1}$, 8.23 $cm^2\ V^{-1}\ S^{-1}$, 6.05 $cm^2\ V^{-1}\ S^{-1}$, and 2.07 $cm^2\ V^{-1}\ S^{-1}$ respectively.

Plotted in Figure 6 is the temperature dependence of the total and lattice contributions to the total thermal conductivity. The inset in (b) is the electronic contribution to the total thermal conductivity. NiSb nanoparticles have increased thermal conductivity in 0.074 and 0.16 NiSb samples. At 325 K,

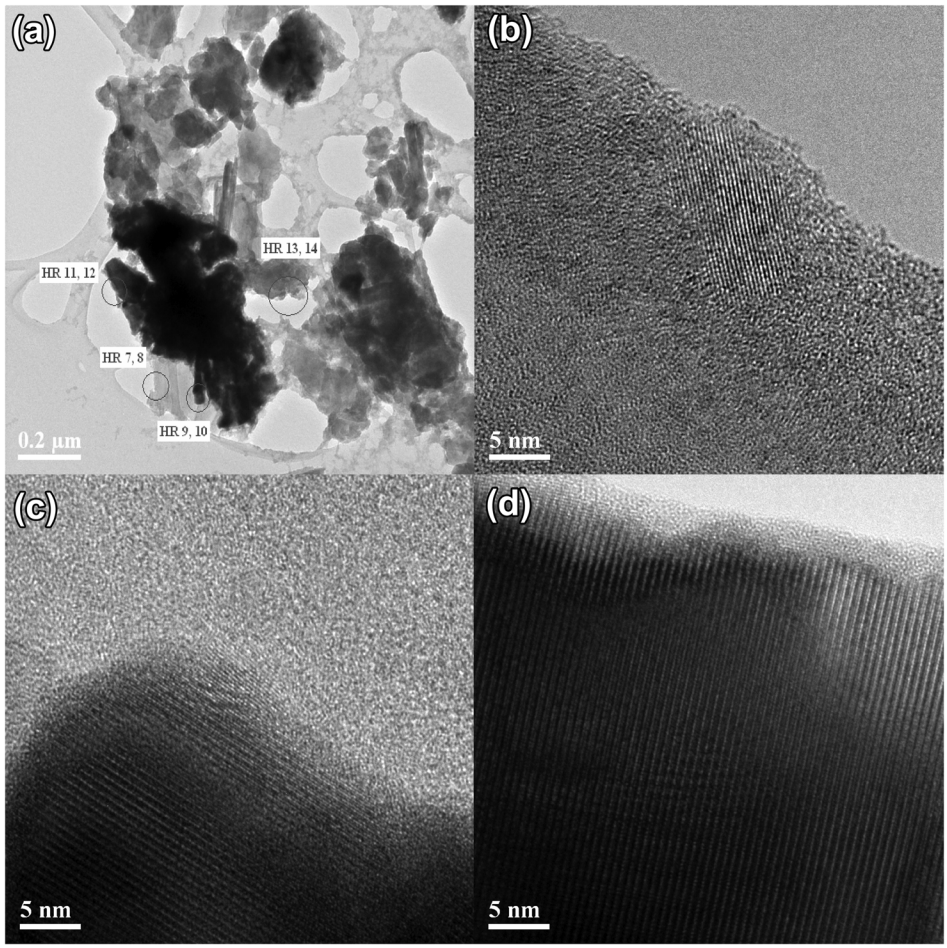

FIG. 3. (a) HRTEM images of the 0.16 sample; (b) displays area 8; (c) and (d) show area 11 and 12 respectively.

0.074 and 0.16 NiSb samples have 5.23 W $m^{-1}K^{-1}$ and 5.7 W $m^{-1}K^{-1}$ respectively, compared to 4.2 W $m^{-1}K^{-1}$ and 3.9 W $m^{-1}K^{-1}$ for bulk and 0.034 samples. One possible reason for the change in thermal conductivity in 0.034 NiSb is the additional role of interfaces in scattering phonons.

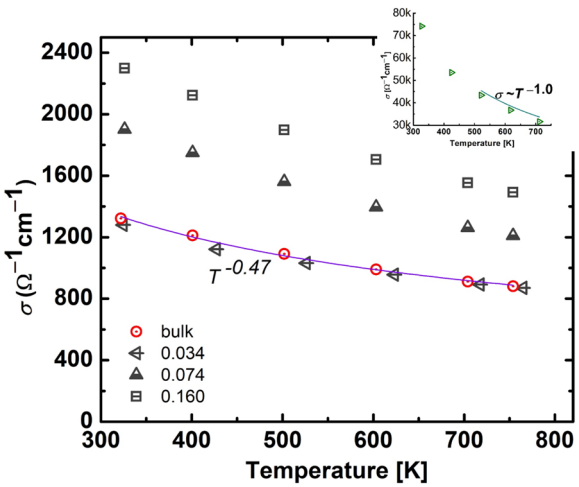

FIG. 4. Temperature dependence of the electrical conductivity of bulk and NiSb composites. Inset shows $\sigma \sim T^{-1.0}$ for pure bulk NiSb (100 μm - 500 μm) synthesized via solid-state reaction.

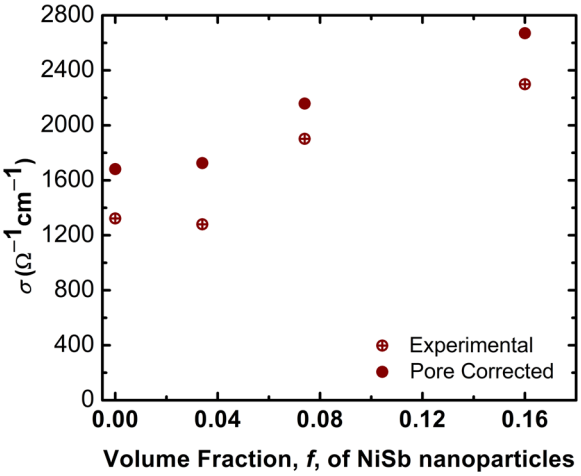

FIG. 5. Experimental and pore corrected electrical conductivity at 322 K.

TABLE II. Experimental and Pore Corrected Electrical Conductivity

f	Experimentalσ_p (Ω^{-1} cm^{-1})	Pore Correctedσ_o (Ω^{-1} cm^{-1})
0 (bulk)	1322.56	1681.69
0.034	1279.65	1725.24
0.074	1901.65	2157.99
0.160	2299.39	2670.1

Randomly formed NiSb layers do not contribute in enhancing phonon scattering due to the interface effect. When the size of the embedded NiSb particle is greater than the phonon wavelength of the bulk material ($Ni_{0.05}Mo_3Sb_{5.4}Te_{1.6}$), the effective thermal conductivity of the composites increases monotonically with respect to the volumetric concentration of highly conducting particles.[35] However, for smaller volume fractions the increase in thermal conductivity is less gradual since the network of highly conducting particles is not formed. As the fraction is increased they form a continuous path between the two ends of the material. These paths are less obstructive for phonons, and thermal conductivity increases more rapidly.[36] In 0.074 and 0.16 NiSb samples a well-connected network of

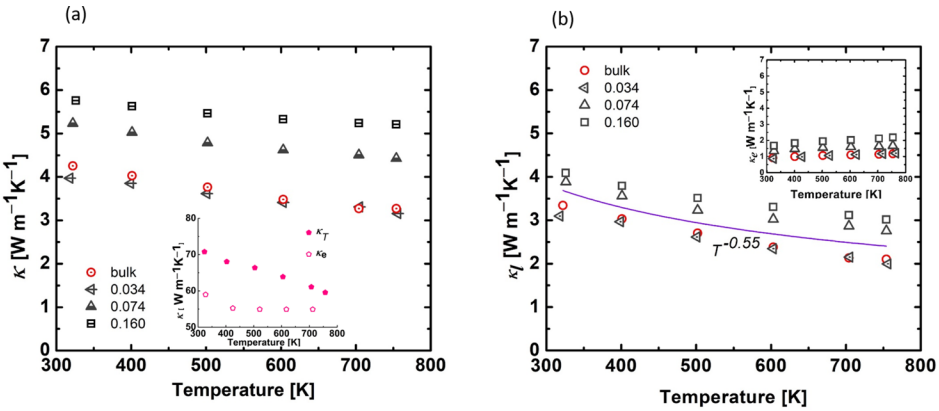

FIG. 6. Temperature dependence of total and lattice thermal conductivity of bulk and NiSb composites. Inset in (a) shows total and electronic thermal conductivity of bulk NiSb synthesizied through solid-state reaction. Inset in (b) shows electronic contribution of thermal conductivity in NiSb composites. Legends for κ_l and κ_e are same.

highly conductive NiSb particles of 70 W $m^{-1}K^{-1}$ [31](6(a) inset) is responsible for the increased thermal conductivity. Among all the samples 0.074 and 0.16 showed less temperature dependence, which is indicative of less inter phonon scattering. In ZnS/diamond composites, the opposite effect was seen.[37] While the 0.4 μm – 4 μm embedded diamond particles (with κ, W $m^{-1}K^{-1}$) increased the composite thermal conductivity, 0.1 μm – 0.5 μm diamond particles have monotonically reduced composite thermal conductivity. Thus, the nature of the interface between the bulk and embedded particle, their thermal conductivity, their acoustic match, physical bonding between them, size of the embedded particles (surface to volume ratio), chemical adherence, and the amount of porosity at the interface play a very important role in deciding the effective thermal conductivity of the composites.[38–40]

Lattice thermal conductivity κ_l was obtained by subtracting κ_e from the total thermal conductivity. κ_e was obtained using Wiedemann-Franz law:

$$\kappa_e = L_o \sigma T \tag{3}$$

Where, L_0 is the Lorenz number, which was obtained using the Seebeck coefficient data assuming our bulk and composites follow a single-parabolic model and multiple scattering mechanisms.[41,42] Temperature dependent Lorenz numbers of bulk and NiSb composites are displayed in Figure 7.

At 325 K, bulk and 0.034 NiSb have a κ_l of 3.3 W $m^{-1}K^{-1}$ and 3.0 W $m^{-1}K^{-1}$ respectively, indicating that NiSb nanoparticles are less effective in preventing phonon contribution to total thermal conductivity. Contrary to this, 0.074 and 0.16 samples have a κ_l of 3.8 W $m^{-1}K^{-1}$ and 4 W $m^{-1}K^{-1}$ respectively. Similarly, for bulk, 0.034, 0.074, and 0.16 samples at 754 K, κ_l values are 2.1 W $m^{-1}K^{-1}$, 1.8 W $m^{-1}K^{-1}$, 2.75 W $m^{-1}K^{-1}$, and 3 W $m^{-1}K^{-1}$ respectively. Since NiSb is metallic in nature, the κ_e contribution to total thermal conductivity is considerable. Included in the Figure 6(b) inset is the contribution of the electronic thermal conductivity to the total thermal conductivity. For bulk and 0.034 samples, the κ_e are almost the same. For rest of the samples the electronic contribution gradually increases, indicating the onset of a different scattering mechanism. Generally, if the umklapp process (inter phonon scattering) is present, lattice thermal conductivity, κ_l, follows $1/T^{\delta}$ with $\delta = 1$. In case of bulk and 0.034 samples δ = -0.55, indicating the low magnitude of the umklapp process. Samples 0.075 and 0.16 also do not show $1/T$ dependence. Similar to our results, Bi nanoparticles (4 wt.%) incorporated into nanostructured PbTe had increased lattice thermal conductivity due to the small acoustic mismatch between Pb and Bi.[21] On the other hand, when micron size $CoSb_3$ polycrystalline particles were nano-plated with nano-size $CoSb_3$ particles there was a considerable reduction in the κ_l.[26]

Pores shape, volume, and probabilistic orientation decide the cross available for heat carrying acoustic waves.[43–45] Similar to electrical conductivity, pore corrected thermal conductivity can be estimated using the following equation:

$$\kappa_p = \kappa_o(1 - P)/(1 + \beta P) \tag{4}$$

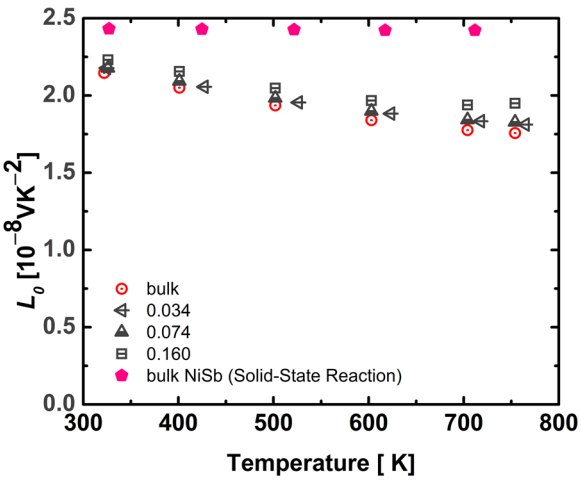

FIG. 7. Temperature dependence of Lorenz numbers.

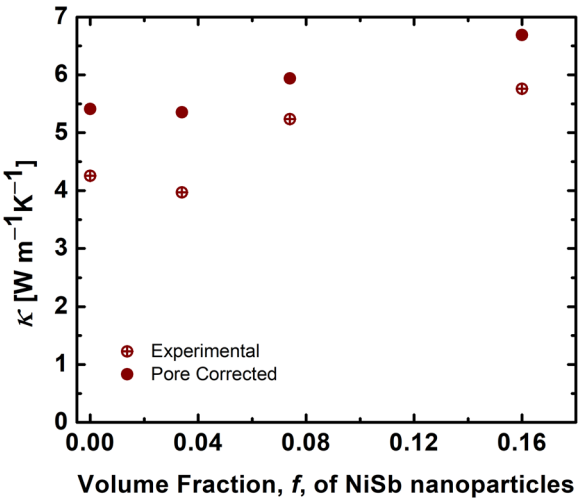

FIG. 8. Experimental and pore corrected thermal conductivity at 322 K.

TABLE III. Experimental and Pore Corrected Thermal Conductivity

f	Experimentalκ_p (W m^{-1}K^{-1})	Pore Correctedκ_o (W m^{-1}K^{-1})
0 (bulk)	4.25	5.41
0.034	3.97	5.35
0.074	5.23	5.94
0.160	5.75	6.68

Where, κ_p is the experimental thermal conductivity with porosity P, κ_o the theoretical thermal conductivity with zero porosity, and $\beta = 2$ for spherical pores. Calculated values are displayed in Figure 8 and Table III. Comparing Table II and Table III, pore corrected thermal conductivity values are similar to pore corrected electrical conductivity in terms of percent reduction. Large differences in the 0.034 NiSb samples is due to its low relative density compared to rest of the samples.

The variations in the Seebeck coefficient with respect to temperature for bulk and various bulk/NiSb composites is shown in Figure 9. The bulk sample has a relatively higher slope than

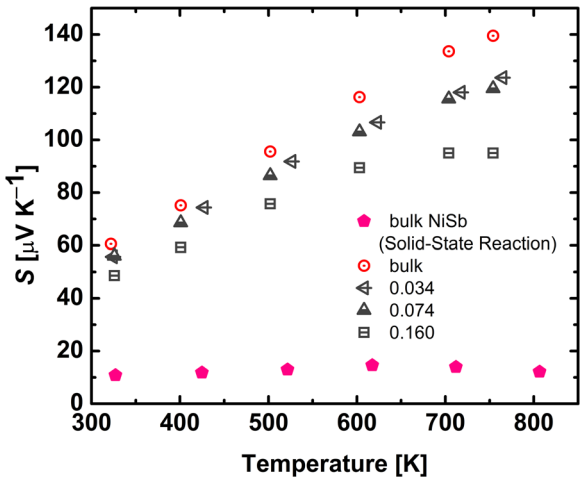

FIG. 9. Temperature dependence of the Seebeck coefficient of bulk, composites and bulk NiSb synthesized through solid-state reaction.

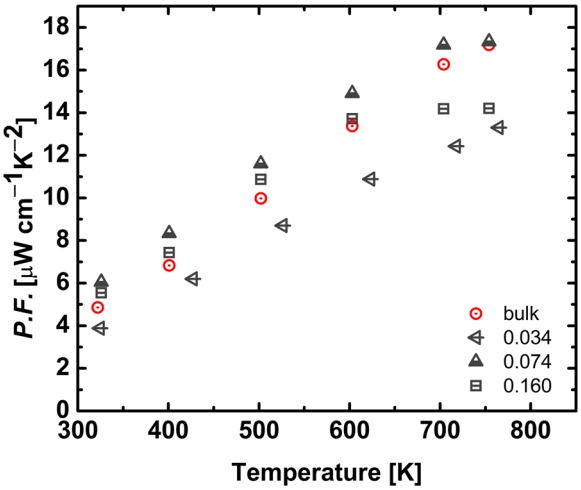

FIG. 10. Temperature dependence of *P.F.* for bulk and NiSb composites.

the rest of the samples. This behavior is a typical for the $Mo_3(Sb,Te)_7$ family of compounds. At 322 K, bulk, 0.034, 0.074 and 0.16 samples have Seebeck coefficients of 60 μV K^{-1}, 55 μV K^{-1}, 56 μV K^{-1}, and 48 μV K^{-1} respectively. Samples 0.034 and 0.074 have the same variation in all the temperature segments. For metals or degenerate semiconductors, the Seebeck coefficient and electrical conductivity have reciprocal relation according Mott[46] and is represented as:

$$S = 8\pi^2 k_B{}^2 m^*/(3eh^2)(\pi/3n)^{2/3} \tag{5}$$

$$\sigma = ne\mu \tag{6}$$

Where k_B, e, h, m^*, n, and μ are the Boltzmann constant, electronic charge, Planck's constant, effective mass of charge carrier, charge carrier concentration, and carrier mobility respectively. Comparing the electrical conductivity of sample 0.074 (1901 Ω^{-1} cm^{-1} at 322 K) to 0.034 (1280 Ω^{-1} cm^{-1} at 322 K), and their respective Seebeck coefficients at the same temperature (55 μV K^{-1} and 56 μV K^{-1}) clearly indicates that in 0.074 NiSb the reciprocal relationship between the electrical conductivity and Seebeck coefficient is decoupled. This kind of behavior has been observed in $Ni_{0.05}Mo_3Sb_{5.4}Te_{1.6}$/MWCNT and *n*-type Skutterudite compounds with MWCNT as nanoinclusions.[6,47] Sample 0.16 has a linear variation in the Seebeck coefficient between 322 K and 600 K. Beyond 600 K, the Seebeck coefficient starts to saturate due to the participation of minority carriers. Since in our samples the diffusive part of the Seebeck coefficient is dominant:

$$S \propto \pi^2 k_B{}^2 T/eE_f \tag{7}$$

Where E_f is the Fermi level and k_B is the Boltzmann constant. The reduction in the slope of S vs. T would indicate a rise in E_f, i.e., with increase in NiSb content in our case. Therefore, 0.034 and 0.074 must have the same E_f. The Seebeck coefficient of bulk NiSb was found to be 10.8 μV K^{-1}at 325 K. It is *p*-type until 700 K and above that exhibits *n*-type behavior.[31] Penn et al. have reported Seebeck values for pure NiSb as ~3 μV K^{-1} at room temperature.[48]

The variation of *P.F.* ($S\sigma^2$) with respect to temperature is similar to the Seebeck coefficient. At 325 K, *P.F.* lies between 4 to 6 μW$cm^{-1}K^{-2}$ for all samples (Figure 10). However, 0.074 NiSb maintains dominance in *P.F.* among all samples from 322 K to 700 K. The main contributing factor to enhanced *P.F.* is elevated electrical conductivity. Competing with this is sample 0.16, but due to the drop in Seebeck coefficient of this sample *P.F.* starts to saturate at 700 K. At 400 K, 500 K, and 600 K, 0.074 NiSb exhibited a 22%, 16%, and 11.3% increase in *P.F.* compared to bulk.

CONCLUSIONS

We have shown that $Ni_{0.05}Mo_3Sb_{5.4}Te_{1.6}$ can be coated with NiSb nanoparticles of 60 nm – 80 nm using a solvothermal nanoplating technique without affecting the bulk material. For samples with

0.074 and 0.16 NiSb particles the electrical conductivity was enhanced, which is the reason the *P.F.* for the 0.074 sample increased by 16%. Between 322 K and 600 K, this sample has the highest power factor among those tested. For the same samples, κ_l and κ_e thermal conductivities were enhanced, whereas for the 0.034 NiSb sample thermal conductivity stayed the same. Electrical conductivity variation in the bulk material and 0.034 NiSb shows alloy scattering ($\sigma \sim T^{-0.5}$) is present in these samples. In the 0.074 NiSb sample the reciprocal relationship between the Seebeck coefficient and the electrical conductivity is broken, giving rise to enhanced *P.F.* The prevention of $NiSb_2$ formation has the potential to improve the TE properties even further. Our study provides an indication that grain boundary manipulation via wet chemistry is indeed an economically viable method to fabricate nanostructured TE materials.

ACKNOWLEDGMENTS

Authors appreciate the Discovery Grant from the Natural Sciences and Engineering Research Council of Canada (NSERC). Also, this work was funded through the Natural Sciences and Engineering Research Council (NSERC) of Canada – Strategic Project Grant (STPGP 430654-12). We would also like to acknowledge the help and assistance provided by the Schwartz-Resiman Foundation under the Waterloo-Technion Research Co-operation Program. The authors declare no competing interests.

[1] H. Kleinke, Chem. Mater. **22**, 604 (2009).
[2] D. M. Rowe and C. M. Bhandari, *Modern Thermoelectrics* (Holt, Rinehart and Winston, London, 1983).
[3] K. Kōmoto and T. Mori, *Thermoelectric Nanomaterials: Materials Design and Applications* (Springer, Berlin, New York, 2013).
[4] W. Liu, H. Shi, H. Ma, and S. B. Tsai, in *Green Production Strategies for Sustainability* (IGI Global, 2018), p. 210.
[5] D. M. Rowe and C. M. Bhandari, Applied Energy **6**, 347 (1980).
[6] N. Nandihalli, S. Gorsse, and H. Kleinke, J. Solid State Chem. **226**, 164 (2015).
[7] N. Nandihalli, A. Lahwal, D. Thompson, T. C. Holgate, T. M. Tritt, V. Dassylva-Raymond, L. Kiss, E. Sellier, S. Gorsse, and H. Kleinke, J. Solid State Chem. **203**, 25 (2013).
[8] W. Liu, X. Yan, G. Chen, and Z. Ren, Nano Energy **1**, 42 (2012).
[9] A. Minnich, M. S. Dresselhaus, Z. Ren, and G. Chen, Energy Environ. Sci. **2**, 466 (2009).
[10] Y. Lan, A. J. Minnich, G. Chen, and Z. Ren, Advanced Functional Materials **20**, 357 (2010).
[11] D. L. Medlin and G. J. Snyder, Curr. Opin. Colloid Interface Sci. **14**, 226 (2009).
[12] L. D. Hicks and M. S. Dresselhaus, Phys. Rev. B: Condens. Matter **47**, 12727 (1993).
[13] J. P. Heremans, C. M. Thrush, and D. T. Morelli, Phys. Rev. B: Condens. Matter **70**, 115334 (2004).
[14] M. S. Dresselhaus, G. Chen, M. Y. Tang, R. Yang, H. Lee, D. Z. Wang, Z. Ren, J. Fleurial, and P. Gogna, Adv. Mater. **19**, 1043 (2007).
[15] J. W. Sharp, S. J. Poon, and H. J. Goldsmid, Physica Status Solidi (A) **187**, 507 (2001).
[16] J. R. Szczech, J. M. Higgins, and S. Jin, J. Mater. Chem. **21**, 4037 (2011).
[17] G. Schierning, Physica Status Solidi (A) **211**, 1235 (2014).
[18] T. Ikeda, L. A. Collins, V. A. Ravi, F. S. Gascoin, S. M. Haile, and G. J. Snyder, Chem. Mater. **19**, 763 (2007).
[19] X. B. Zhao, X. H. Ji, Y. H. Zhang, and B. H. Lu, J. Alloys Compd. **368**, 349 (2004).
[20] Y. H. Zhang, T. J. Zhu, J. P. Tu, and X. B. Zhao, Mater. Chem. Phys. **103**, 484 (2007).
[21] J. R. Sootsman, R. J. Pcionek, H. Kong, C. Uher, and M. G. Kanatzidis, Chem. Mater. **18**, 4993 (2006).
[22] X. Ji, B. Zhang, Z. Su, T. Holgate, J. He, and T. M. Tritt, Physica Status Solidi. A, Applied research **206**, 221 (2009).
[23] B. Zhang, J. He, X. Ji, T. M. Tritt, and A. Kumbhar, Appl. Phys. Lett. **89**, 163114 (2006).
[24] P. N. Alboni, X. Ji, J. He, N. Gothard, and T. M. Tritt, Appl. Phys. Lett. **103**, 113707 (2008).
[25] X. Ji, J. He, Z. Su, N. Gothard, and T. M. Tritt, J. Appl. Phys. **104**, 034907 (2008).
[26] X. Ji, J. He, P. Alboni, Z. Su, N. Gothard, B. Zhang, T. M. Tritt, and J. W. Kolis, Physica Status Solidi (RRL)-Rapid Research Letters **1**, 229 (2007).
[27] P. Alboni, X. Ji, J. He, N. Gothard, and T. M. Tritt, J. Appl. Phys **103**, 113707 (2008).
[28] N. Nandihalli, Q. Guo, S. Gorsse, A. Khan, T. Mori, and H. Kleinke, Eur. J. Inorg. Chem. **2016**, 853 (2016).
[29] L. Kumari, W. Li, J. Y. Huang, and P. P. Provencio, J. Phys. Chem. C **114**, 9573 (2010).
[30] C. Li, J. Hu, Q. Peng, and X. Wang, Mater. Chem. Phys. **110**, 106 (2008).
[31] N. Nandihalli, Doctoral Thesis, University of Waterloo, Waterloo, Canada, 2016.
[32] W. J. Parker, R. J. Jenkins, C. P. Butler, and G. L. Abbott, J. Appl. Phys. **32**, 1679 (1961).
[33] H. Xu, K. M. Kleinke, T. Holgate, D. Rossouw, G. Botton, T. M. Tritt, and H. Kleinke, J.Alloys Compd. **504**, 314 (2010).
[34] X. Shi, Y. Pei, G. J. Snyder, and L. Chen, Energy Environ. Sci. **4**, 4086 (2011).
[35] W. Tian and R. Yang, Computer Modeling in Engineering and Sciences **24**, 123 (2008).
[36] D. Stauffer and A. Aharony, *Introduction to percolation theory* (CRC press, 1994).
[37] A. G. Every, Y. Tzou, D. Hasselman, and R. Raj, Acta Metall. Mater. **40**, 123 (1992).
[38] H. Bhatt, K. Y. Donaldson, D. Hasselman, and R. T. Bhatt, J. Am. Ceram. Soc. **73**, 312 (1990).
[39] D. Hasselman, K. Y. Donaldson, and A. L. Geiger, J. Am. Ceram. Soc. **75**, 3137 (1992).
[40] D. ter Haar, *Collected Papers of P.L. Kapitza*, Vol. 2 (Pergamon Press, Oxford, 1965).
[41] Q. Guo and H. Kleinke, J. Solid State Chem. **215**, 253 (2014).

[42] V. I. Fistul and J. Blakemore, *Heavily doped semiconductors* (Plenum Press, New York, 1969).
[43] J. Francl and W. D. Kingery, J. Am. Ceram. Soc. **37**, 99 (1954).
[44] L. Yang, J. Wu, and L. T. Zhang, J. Alloys Compd. **364**, 83 (2004).
[45] D. S. Smith, S. Fayette, S. Grandjean, C. Martin, R. Telle, and T. Tonnessen, J. Am. Ceram. Soc. **86**, 105 (2003).
[46] N. F. Mott and H. Jones, *The theory of the properties of metals and alloys* (Courier Corporation, 1958).
[47] T. Itoh, K. Ishikawa, and A. Okada, Journal of Materials Research **22**, 249 (2007).
[48] J. Penn and E. Miller, J. Appl. Phys. **44**, 177 (1973).